Organic & Biomolecular Chemistry

ROYAL SOCIETY OF CHEMISTRY

PAPER

View Article Online
View Journal | View Issue

Cite this: *Org. Biomol. Chem.*, 2023, **21**, 5648

Photo-induced crosslinking uncovers an antiparallel strand orientation in heterodimeric $(EIAALEK)_3/(KIAALKE)_3$ and $(EIAALEK)_3/(RIAALRE)_3$ coiled-coil systems†

D. Aerssens,‡[a] L. Miret-Casals, *‡[a] D. Gomez,[b] D. Sousa-Neves,[a] Y. Levy, [c] M. De Vleesschouwer,[a] A. Manicardi *[a,d] and A. Madder *[a]

Received 30th November 2022,
Accepted 20th June 2023

DOI: 10.1039/d2ob02181a

rsc.li/obc

We describe for the first time the co-existence of the parallel and antiparallel conformation of the heterodimeric E3/K3 and E3/R3 coiled-coil systems in solution. The introduction of a furanylated amino acid in the $(EIAALEK)_3$ sequence allowed, upon photo-induced covalent crosslinking, freezing of the respective coiled-coil complexes present in solution. The occurrence of both parallel and antiparallel conformations in solution was supported by computational simulations and further confirmed by fluorescence experiments based on pyrene–pyrene stacking.

Introduction

In 1953, Crick and Pauling described, independently from each other, for the first time the coiled-coil peptide structure in detail.[1–3] The α-helical coiled-coil is by far the most well-understood and most widely occurring protein-folding motif. As a result, sequence-to-structure relationships are available for the prediction of natural coiled-coil sequences and have fuelled the *de novo* design of proteins featuring unnatural sequences and unprecedented properties based on physical principles of intramolecular and intermolecular interactions.[4–6] To design a dimeric coiled-coil motif, researchers make use of H (hydrophobic) and P (polar) residues that follow the HPPHPPP pattern.[7]

However, it was demonstrated that the structure predicted according to theory and computational calculations is not always in line with the actual crystal structure. This is due to a lack of understanding, at the atomic level, of the detailed physicochemical features that kinetically and thermodynamically direct the formation of a unique, cooperatively folded, native structure. For instance, the poly-heptapeptide sequence, designed by Hodges,[8] which was intended to mimic the two-stranded coiled-coil conformation of tropomyosin, a protein that regulates actin filament functions,[9] was modified and used as a model system by O'Neil for evaluating the helix-forming tendencies of the 20 amino acids.[10] Later, X-ray data revealed that a triple-stranded coiled-coil, formed by three alpha-helices, was formed instead of the expected dimeric coiled-coil.[11] As an additional example, for the alpha1 peptide designed by Hill, which was conceived to form a 4-helix bundle, co-existence of a tetrameric and a hexameric structure was shown upon analysis of the X-ray crystal structure.[12] While the coiled-coil motif appears rather simple, a surprising diversity of final adopted structures can be observed when considering all design efforts that have been described over the last decades. Coiled-coils can consist of two to seven α-helices that may be arranged in a parallel (all peptides oriented from N → C) or antiparallel (peptides oriented N → C and C → N) manner.[7,13,14] Additionally, those helices can be identical or different, resulting in homomers or heteromers.[7,15] Furthermore, larger structures such as the α-sheets and α-cylinders, described by Walshaw and Woolfson, may be formed due to the supramolecular assembly of different coiled-coils.[16]

One of the most exploited systems, originally described by Litowski and Hodges, is the heterodimeric $(EIAALEK)_3/(KIAALKE)_3$ coiled-coil system (E3/K3 coiled-coil).[17] Although the sequences are relatively short, the complex shows stability in the nanomolar range (K_D = 70 nM).[17] This high preference to pair with one another *via* intermolecular interactions, is often referred to as Molecular Velcro.

[a]*Organic and Biomimetic Chemistry Research Group, Department of Organic and Macromolecular Chemistry, Ghent University, Krijgslaan 281-S4, Gent 9000, Belgium. E-mail: Annemieke.madder@ugent.be, Alex.Manicardi@unipr.it, Laia.MiretCasals@ugent.be*
[b]*Department of Biology and Chemistry, New York University, New York 10003, USA*
[c]*Department of Structural Biology, Weizmann Institute of Science, Rehovot, Israel*
[d]*Department of Chemistry, Life Sciences and Environmental Sustainability, University of Parma, Viale delle Scienze, 17/A, I-43124 Parma, Italy*

†Electronic supplementary information (ESI) available. See DOI: https://doi.org/10.1039/d2ob02181a

‡First author.

While not as versatile as nucleic acid duplex recognition and duplex formation in terms of the number of potential complementary sequences, coiled-coil peptides have a high sequence selectivity and can be easily genetically encoded into the protein of interest.[18] In this way, the incorporation of one coil partner sequence into a biomolecule allows hybridization with a suitably designed and modified partner coil.[18] Such strategies open routes toward a broad range of applications including, among others biosensors,[19,20] templated ligation reactions,[21] fluorescent labelling of membrane embedded-proteins,[22–25] drug delivery systems,[26] and detection of receptor dimerization.[27,28] It is evident that in such strategies fine-tuned control over the strand orientation of the coiled-coils (*i.e.* parallel or antiparallel) is of utmost importance and determines the success of the final application and the sensitivity of the designed detection methods.[24–27,29,30]

However, the stabilities of such non-covalent intermolecular interactions are dependent on the concentration and are directly proportional to the number of heptad repeats and the correct pairing of the hydrophobic and electrostatic interactions. Therefore, Molecular Velcro applications based on the formation of a covalent bond between both coils were developed to provide more stability to minimal coiled-coils and can be useful for subsequent biochemical analysis.[31–33]

Noticeably, previously described applications are based on the principle that mixing the original unmodified K-and E-coil containing entities results in a parallel coiled-coil orientation.[25,31,34] Traditionally, techniques such as X-ray crystal structure determination,[35] disulfide exchange,[36] fluorescence quenching,[37] NMR,[38] paramagnetic NMR spectroscopy,[39] and double electron–electron resonance spectroscopy have been used to confirm the strand orientation within coiled-coil complexes.[40] However, alternative coiled-coil conformations existing in solution can be overlooked if, for example, the strand orientation is determined by XRD and there is a difference in solubility between the parallel and antiparallel coiled-coil complexes, leading to misinterpretations.

In the current work, we explore the use of furan-oxidation crosslink technology to generate covalently crosslinked coiled-coils, as a means to trap and study the orientation of the $(EIAALEK)_3$/$(KIAALKE)_3$ (E3/K3) coiled-coils. It was shown that next to the classical parallel conformation, the antiparallel conformation of the heterodimeric E3/K3 coiled-coil system was also present in solution.

Results and discussion

Photo-induced furan oxidation has been used for crosslinking and labelling purposes in a variety of biomolecular interaction studies within our research group.[41] The strength of this crosslink strategy lies in the fact that furan can be considered a warhead that can be triggered into a keto-enal, in a selective and spatiotemporally controlled way, upon the production of singlet oxygen by light irradiation in the presence of photosensitizers.[42] This furan-oxidation strategy has been successfully applied in the context of DNA, RNA, or PNA interstrand crosslinking,[42–45] covalent linkage of ligands to cell-surface receptors,[46] and crosslinking of complementary protein partners.[47]

More recently, we equipped a heterodimeric E3/R3 (with arginines replacing lysines) coiled-coil system with an E_{coil} furan warhead to identify new nucleophilic R_{coil} located partners for the electrophile generated upon furan oxidation. We demonstrated that besides lysine, also cysteine and tyrosine are potential nucleophilic partners able to react with the furan moiety and form a covalent bond.[48]

In the current study, the heterodimeric E3/K3 coiled-coil was used to investigate the behaviour of a furan-modified E_{coil} to crosslink to the natural K_{coil}, which contains six lysine residues. Each coil peptide is composed by three heptad repeats (3 × gabcdef, Fig. 1A) of seven amino acids with hydrophobic contacts at the a (isoleucine, I) and d positions (leucine, L) that establish the hydrophobic core. Ionic residues at the e and g position (glutamic acid, E for the E_{coil} and lysine, K for the K_{coil}) ensure charge complementarity of the coils. To evaluate the influence of chain length of the furan moiety on crosslinking to lysine, next to the introduction of FuA (2-furylalanine), also Dap (2,3-diaminopropionic acid), Dab (2,4-diaminobutyric acid), Orn (ornithine), and Lys (lysine) were introduced at position 8 of the E_{coil} as handles to couple the Fur moiety (see Fig. 1B). In addition, an Aba (4-acetamidobenzoic acid) moiety was introduced at the N-terminus to ensure sufficient UV-activity for HPLC detection and an amide group at the C-terminus to minimize any repulsive electrostatic interactions between the E3/K3 coils (see Table 1).

From previous work, it is known that introducing a modified amino acid at the ionic residue positions (*e* and *g* position in the helical wheel representation, Fig. 1A) does not interfere with the formation of a classical helical coiled-coil structure.[48] The K_{coil}, E_{coil}-FuA-8, and E_{Coil}-X_{Fur}-8 were synthesized (Table 1 and data in ESI, Fig. S1–7†). In addition, the CD spectra of the E3/K3 coiled-coils were recorded and demonstrate that coiled-coil domains are formed with the characteristic minima at 208 and 222 nm as previously reported for the heterodimeric E3/K3 coiled-coil model system (data in ESI, Fig. S8†).[17]

Next, crosslink experiments were performed by pre-incubating both coils to allow coiled-coil formation followed by light irradiation in the presence of Rhodamine B (Rho B), a photosensitizer, to produce singlet oxygen (Fig. 1C). Indeed, broadened and/or multiple peaks corresponding to crosslinked species (as deduced from HPLC and MS analysis) were observed for all E_{Coil}-X_{Fur}-8 in the obtained chromatograms (see Fig. 2 and data in ESI, Fig. S 9 and 10†). This is an indication of the formation of several crosslink products (see red dots in Fig. 2) resulting from the attack of different lysine residues in the K_{coil} onto the activated furan moiety in the E_{coil}. The analytical data for the crosslinked products are in accordance with the formation of a 4-ketoamide structure (Fig. 1C) and its dehydrated (−18 Da) and oxidised (+16 Da) form, as previously reported[47,48] (data in ESI, Fig. S10†). Note that no crosslinked product is observed for E_{Coil}-FuA-8, bearing the shortest side-chain (Fig. 2A).

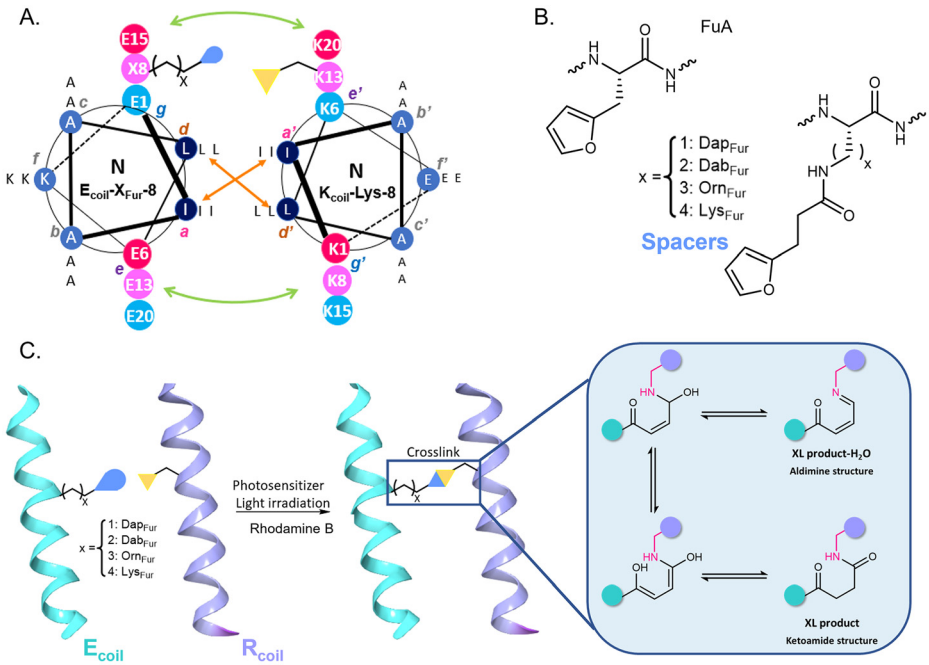

Fig. 1 (A) Helical wheel representation of the heterodimeric E3/K3 coiled-coil dimer. The green arrows indicate electrostatic interactions whereas the orange arrows indicate hydrophobic interactions. (B) Structure of the furanylated amino acids featuring spacers of different lengths between furan and the peptide backbone. (C) Representation of the E_{coil} (light blue) obtained after introduction of one of the furanylated amino acids, the R_{coil} (purple), and the possible structures obtained after crosslinking. The furan moiety is introduced in the E_{coil} using the 2-furylalanine or through reaction of 3-(2-furyl)propionic acid with the side chain amino group of 2,3-diaminopropionic acid (Dap), 2,4-diaminobutyric acid (Dab), ornithine (Orn), or lysine (Lys).

Table 1 Overview of the K_{coil}, E_{coil}, E_{coil}-FuA-8, and E_{coil}-X_{Fur}-8 sequences. Aba: 4-acetamidobenzoic acid; FuA: 2-furylalanine, Dap: 2,3-diaminopropionic acid; Dab: 2,4-diaminobutyric acid; Orn: ornithine; Lys: lysine, Fur: 3-(2-furyl)propionic acid that reacted with the side chain amino group

Name	Peptide sequence
K_{coil}	Aba-KIAALKEKIAALKEKIAALKE-NH_2
E_{coil}	Aba-EIAALEK-**E**-IAALEKEIAALEK-NH_2
E_{coil}-FuA-8	Aba-EIAALEK-**FuA**-IAALEKEIAALEK-NH_2
E_{coil}-Dap_{Fur}-8	Aba-EIAALEK-**Dap$_{(Fur)}$** -IAALEKEIAALEK-NH_2
E_{coil}-Dab_{Fur}-8	Aba-EIAALEK-**Dab$_{(Fur)}$** -IAALEKEIAALEK-NH_2
E_{coil}-Orn_{Fur}-8	Aba-EIAALEK-**Orn$_{(Fur)}$** -IAALEKEIAALEK-NH_2
E_{coil}-Lys_{Fur}-8	Aba-EIAALEK- **Lys$_{(Fur)}$** -IAALEKEIAALEK-NH_2

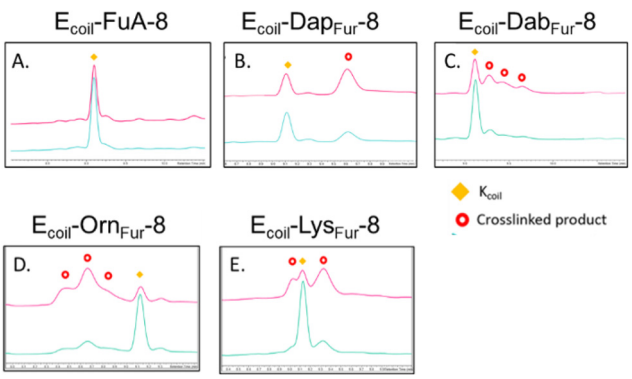

Fig. 2 Zooms of HPLC-UV chromatograms focussed on the K_{coil} and crosslinked products region recorded at 260 nm. The reaction mixture after light irradiation (pink trace) results from the crosslink reaction between K_{coil} at 5 μM and (A) E_{coil}-FuA-8 (B) E_{coil}-Dap_{Fur}-8 (C) E_{coil}-Dab_{Fur}-8 (D) E_{coil}-Orn_{Fur}-8 and (E) E_{coil}-Lys_{Fur}-8 at 10 μM after 60 minutes of light irradiation with Rho B at 10 μM. The green trace represents the mixture containing both E_{coil}-X_{Fur}-8 and K_{coil} peptides as well as Rho B at t = 0.

To identify which lysine-side chains can present a suitably oriented nucleophilic amine and engage in crosslinking, we designed a 'lysine scan' experiment by synthesizing a series of R_{coil} peptides where all lysines of the original K_{coil} but one are replaced with arginines. The resulting peptides are referred to as R_{coil}-Lys-X peptides, where X refers to the position of the unique lysine residue in the sequence (Table 2 and data in ESI Fig. S11–16†). All R_{coil}-Lys-X peptides were subsequently used to study the crosslinking behavior of E_{coil}-Dap_{Fur}-8 and E_{coil}-Orn_{Fur}-8 peptides, which were selected because baseline separated peaks are obtained (crosslinked product from the K_{coil} peak in the chromatogram) when crosslinked with K_{Coil} (Fig. 2, compare panel C and E with B and D).

E_{coil}-Dap_{Fur}-8 can crosslink to R_{coil}-Lys-8 and R_{coil}-Lys-13 (data in ESI, Fig. S17 and 18†), whereas E_{coil}-Orn_{Fur}-8 can additionally crosslink to R_{coil}-Lys-6 and R_{coil}-Lys-15 (data in ESI, Fig. S19–22†). The longer spacer present in the Orn residue as opposed to the Dap residue can explain this observed difference in reactivity.

Table 2 Overview of the K_{coil}, R_{coil}-Lys-*X*, and E_{coil}-Dap_{Fur}-*X* sequences. Aba: 4-acetamidobenzoic acid; Dap: 2,3-diaminopropionic acid; Lys: lysine; Fur: 3-(2-furyl)propionic acid that reacted with the side chain amino group

Name	Peptide sequence
K_{coil}	Aba-KIAALKEKIAALKEKIAALKE-NH_2
R_{coil}-Lys-1	Aba-KIAALRERIAALRERIAALRE-NH_2
R_{coil}-Lys-6	Aba-**R**IAALKE**R**IAALRE**R**IAALRE-NH_2
R_{coil}-Lys-8	Aba-**R**IAALRE**K**IAALRE**R**IAALRE-NH_2
R_{coil}-Lys-13	Aba-**R**IAALRE**R**IAALKE**R**IAALRE-NH_2
R_{coil}-Lys-15	Aba-**R**IAALRE**R**IAALRE**K**IAALRE-NH_2
R_{coil}-Lys-20	Aba-**R**IAALRE**R**IAALRE**R**IAALKE-NH_2
E_{coil}-Dap_{Fur}-1	Aba-**Dap$_{(Fur)}$**-IAALEKEIAALEKEIAALEK-NH_2
E_{coil}-Dap_{Fur}-6	Aba-EIAAL-**Dap$_{(Fur)}$**-KEIAALEKEIAALEK-NH_2
E_{coil}-Dap_{Fur}-8	Aba-EIAALEK-**Dap$_{(Fur)}$**-IAALEKEIAALEK-NH_2
E_{coil}-Dap_{Fur}-13	Aba-EIAALEKEIAAL-**Dap$_{(Fur)}$**-KEIAALEK-NH_2
E_{coil}-Dap_{Fur}-15	Aba-EIAALEKEIAALEK-**Dap$_{(Fur)}$**-IAALEK-NH_2
E_{coil}-Dap_{Fur}-20	Aba-EIAALEKEIAALEKEIAAL-**Dap$_{(Fur)}$**-K-NH_2

In literature studies, the E3/K3 coiled-coil system and variations thereof are reported to be almost exclusively parallel.[38–40] However, as can be intuitively observed from the helical wheel presentation (Fig. 1A), a parallel coiled-coil orientation does not allow explaining why the E_{coil}-Dap_{Fur}-8 and E_{coil}-Orn_{Fur}-8 peptides can crosslink to the R_{coil}-Lys-8 peptide, nor how crosslinking can occur between the E_{coil}-Orn_{Fur}-8 and R_{coil}-Lys-15 peptides. Indeed, the reacting residues are located at opposite sides of the coiled-coil complex, which indicates the possible co-existence of an antiparallel E3/R3 coiled-coil conformation.

In order to further confirm this unexpected behaviour and to further study the strand orientation of the E3/R3 coiled-coil system (parallel and antiparallel orientation), a new series of E_{coil}-Dap_{Fur}-*X* peptides, in which one Glu was replaced by a Dap_{Fur} at positions 1, 6, 13, 15, or 20, were synthesized (Table 2 and data in ESI, Fig. S23–27†). Dap_{Fur} was exploited for its shorter side chain and concurrent higher selectivity of crosslinking. Subsequently, a series of crosslinking experiments were performed using all possible combinations of E_{coil}-Dap_{Fur}-*X* and R_{coil}-Lys-*X* peptides (data in ESI, Fig. S28–39† show experiments where crosslinked product is observed). Remarkably, each E_{coil}-Dap_{Fur}-*X* peptide can crosslink with two R_{coil}-Lys-*X* peptides (see Fig. 3C, colored boxes).

Since proximity is pivotal for crosslinking, the observed crosslinking behaviour can only be explained by assuming that the heterodimeric E3/R3 coiled-coils can adopt a parallel (see rich colors in Fig. 3A) as well as an antiparallel (see faded colors in Fig. 3B) orientation in solution. The table in Fig. 3C summarizes the crosslink results and shows the yields of the crosslinked products. Note that when the Fur moiety within the E_{coil} as well as the Lys residue within the R_{coil} are incorporated at the original locations of the ionic residues of the second heptad repeat (E_{coil}-Dap_{Fur}-8/13 and R_{coil}-Lys-8/13), higher crosslink yields are obtained (Fig. 3C). In addition, the CD spectra of the E_{coil}-Dap_{Fur}-13 with R_{coil}-Lys-8 (which should adopt a parallel strand orientation to allow crosslink) and E_{coil}-Dap_{Fur}-13 with R_{coil}-Lys-13 (which should adopt an antiparallel strand orientation to allow crosslink) were recorded and demonstrate that coiled-coil domains are formed (data in ESI, Fig. S40†). These results suggest that there is a co-existence of parallel and antiparallel strand orientations in the E3/R3 coiled-coil system and the furan-oxidation crosslink technology allows trapping both conformations. Note that CD spectra for the other combinations between E_{coil}-Dap_{Fur}-13 and R_{coil}-Lys-*X*, where crosslinked products were not observed, also show CD signatures corresponding to coiled-coil formation (see data in ESI, Fig. S40†).

Previously, Franziska Thomas *et al.* also noticed the co-existence of both parallel and antiparallel orientations of their *de novo* designed coiled-coil peptides during a disulfide exchange experiment.[36] By incorporating an Asn residue at the central position of the coil strand, unambiguous parallel assemblies were obtained. As only traces of antiparallel species were detected *via* disulfide exchange experiments of the original coiled-coil system, no detailed analyses were carried out.

In general, the appearance of antiparallel coiled-coil systems is far less common in nature than observation of the corresponding parallel counterparts. Therefore, researchers are devoting special efforts to developing and stabilizing antiparallel heterodimeric coiled-coil systems. More specifically, an antiparallel conformation can be obtained by inverting the sequence or by introducing minor structural changes to the hydrophobic core of the heterodimeric coil $(EXYZLEK)_3$/$(KXYZLKE)_3$ (with X = Val, Ile or Asn, Y = Ser, Ala or Gln, Z = Ala or Gln).[49–52] Additionally, antiparallel motifs can be stabilized by replacing an interhelical salt bridge with a covalent bond, making use of bis-triazole, glycol, and dibenzyl ether linkers.[53]

However, while on one occasion it was reported that for more advanced systems based on designed coiled-coil motifs expectations in terms of conformational behaviour are not always met,[51] more specifically for the often used non-modified heterodimeric $(EIAALEK)_3$/$(KIAALKE)_3$ coiled-coil system, evidence for such co-existence of parallel and antiparallel conformations in solution is, to our knowledge, still missing.

Therefore, the obtained results as shown in Fig. 3 were further validated by computational studies. Using a coarse-grained model, various parallel and antiparallel complexes of the heterodimeric E3/R3 coiled-coil were studied. In the coarse-grained model each amino acid residue is represented by two beads at the Cα and Cβ atoms, allowing significant reduction of the simulation times.

In addition, this representation does not differentiate Arg from Lys, so the simulation is valid for both the E3/R3 and E3/K3 coiled-coil. Furthermore, the coiled-coil is simulated by a native topology-based model that uses the Lennard-Jones potential to represent native contact interactions (see details in ESI, section 11†).[54] All simulations were run for a total number of 3×10^5 steps. Every 1000 steps a snapshot of the coiled-coil configuration was taken. Each helix consists of three heptad repeats, and the distances between the hydrophobic cores (the a–a′/d–d′ positions for the parallel coiled-coil and a–d′/d–a′

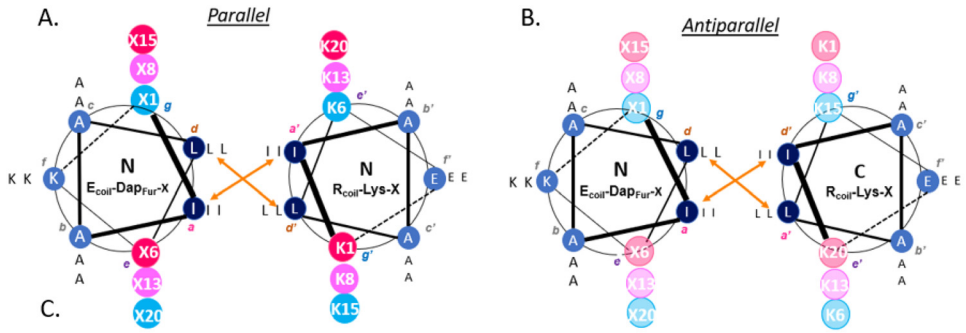

C.

K_n \ X_n	E_{coil}-Dap_{Fur}-1	E_{coil}-Dap_{Fur}-6	E_{coil}-Dap_{Fur}-8	E_{coil}-Dap_{Fur}-13	E_{coil}-Dap_{Fur}-15	E_{coil}-Dap_{Fur}-20
R_{coil}-Lys-1	n.d	27%	n.d	n.d	38%	n.d
R_{coil}-Lys-6	20%	n.d	n.d	n.d	n.d	39%
R_{coil}-Lys-8	n.d	n.d	53%	56%	n.d	n.d
R_{coil}-Lys-13	n.d	n.d	40%	59%	n.d	n.d
R_{coil}-Lys-15	45%	n.d	n.d	n.d	n.d	24%
R_{coil}-Lys-20	n.d	28%	n.d	n.d	36%	n.d

Fig. 3 (A) Helical wheel representation of the parallel orientation of the E_{coil} and R_{coil}. (B) Helical wheel representation of the antiparallel orientation of the E_{coil} and R_{coil}. In both A and B, the orange arrows represent the hydrophobic interactions. Herein, X in the colored circles refers to the classical E_{coil} residues (see Table 2), which are substituted by Dap_{Fur} in a specific position as indicated in the table in panel C. In the R_{coil} all lysines except one (see table in panel C for exact location) are replaced by arginines. (C) Yields for each crosslinked product obtained from the given peptide combinations after 1 h of irradiation with Rho B. The concentration of each E_{coil} peptide was 10 μM and the concentration of the R_{coil} peptides equalled 5 μM. N.d.: not detected. The rich colors in the table refer to yields corresponding to parallel coiled-coils whereas the faded colors are related to yields for anti-parallel coiled-coils. Yields were calculated by integrating signals in the HPLC chromatograms in Fig. S28–39 according to the procedure defined in ESI section 1.5.1.†

positions for the antiparallel coiled-coil, see orange arrows in Fig. 3A and B) were kept constant while still allowing for limited spontaneous sliding of the coiled-coils at the hydrophobic core interface. Additionally, the dynamics of coiled-coil sliding resulting from variable electrostatic interactions, which play a fundamental role in long coiled-coils,[54] were not considered in our system, since the obtained coiled-coils with less than three heptads are generally not stable.[55,56] Furthermore, the covalent bond formed between the oxidized furan on the E_{coil} and the lysine residue on the complementary strand is represented by a general linker, which was placed between the g_i and e'_i position at the E and R_{coil}, respectively, i referring to one of the three heptad repeats in our model. Equivalent positions can be found at the e_i and g'_i locations on the parallel conformation. For the antiparallel conformation, the linker was introduced at the g_i–g'_i positions, which are equivalent to the e_i–e'_i positions. In view of the structural similarities between both sides of the coiled-coil, the studies were only performed on the E_{coil}-Dap_{Fur}-1/R_{coil}-Lys-6/15, E_{coil}-Dap_{Fur}-8/R_{coil}-Lys-13/8 and E_{coil}-Dap_{Fur}-15/R_{coil}-Lys-20/1 coiled-coil combinations (see Fig. 3A and B, upper sides of the helical wheels).

A parallel coiled-coil model of E_{coil}-Dap_{Fur}-1/R_{coil}-Lys-6 was constructed (see Fig. 4). The probability densities between the Cα atoms of the a_i–a'_i residues were plotted against the distance and snapshots of the coiled-coil simulations are included in Fig. 4A. Each of the heptad repeats is colored in a different color: light orange (1st heptad), cyan (2nd heptad), and pink (3rd heptad). The a_i–a'_i pair results are represented in the snapshots as blue (a_1–a_1), magenta (a_2–a_2), and green (a_3–a_3) bars. The furan–lysine linkage is shown as two red beads. In this parallel coiled-coil orientation, the probability density exhibits a maximum at low distances, indicating that the parallel orientation is stable. Next, the corresponding simulation for the antiparallel coiled-coil model of E_{coil}-Dap_{Fur}-1/R_{coil}-Lys-6 was performed (see Fig. 4B). The probability density of a_1–a'_1 (blue) exhibits a maximum at short distances due to the constraint set by the furan–lysine linkage. On the other hand, the probability densities for the other two pairs a_2–a'_2 (magenta) and a_3–a'_3 (green) peak occur at longer distances, indicating that the antiparallel configuration is not stable for this coiled-coil, as shown in Fig. 4B. The same results were obtained for the E_{coil}-Dap_{Fur}-8/R_{coil}-Lys-13 and E_{coil}-Dap_{Fur}-15/R_{coil}-Lys-20 coiled-coils (see Fig. S42†). To support that the parallel model is the preferred configuration for the aforementioned pair, we plot in Fig. 4C the probability density of the number of native contacts Q in the parallel and antiparallel coiled-coil system. In this representation, large Q values represent a folded coiled-coil with a high number of hydrophobic interactions (a_i–a'_i and the d_i–d'_i for parallel and a_i–d'_i and d_i–a'_i pairs for antiparallel) and, therefore, a strong interface (see Fig. S41†). Low Q values represent a coiled-coil with weak hydrophobic inter-

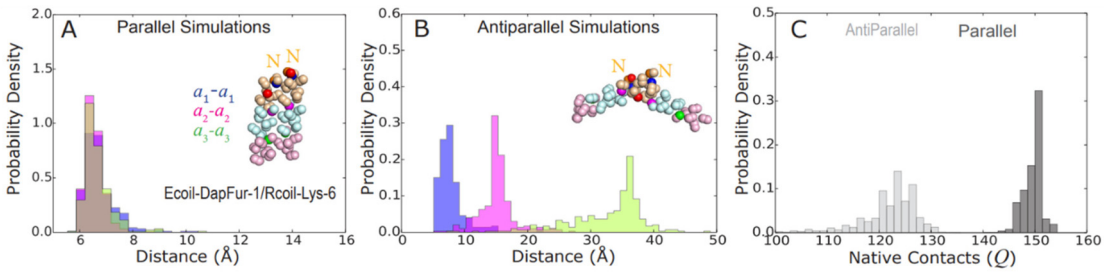

Fig. 4 (A) Probability densities of the distance between the Cα atoms of the a_i–a'_i pairs, with i one of the three heptad repeats of the coiled-coil (CC) model in parallel orientation. (B) Antiparallel version of the CC model. Snapshots of the simulations are shown in panels A and B. Each heptad repeat of the CCs is coloured in a different color: light orange (1st heptad), cyan (2nd heptad), and pink (3rd heptad). The a_i–a_i pair results are represented in the snapshots as blue, magenta, and green bars, respectively. The furan–lysine linkage is represented by the red beads. (C) Probability densities of the number of native contacts *Q*.

actions, indicating poor stability of those configurations. Since the probability density of contacts is higher in the parallel configuration, it can be concluded that the parallel configuration is indeed the preferred state for the E_{coil}-Dap_{Fur}-1/R_{coil}-Lys-6 (see Fig. 4C). The same results were also observed for E_{coil}-Dap_{Fur}-8/R_{coil}-Lys-13 and E_{coil}-Dap_{Fur}-15/R_{coil}-Lys-20 coiled-coils (see Fig. S42†).

Next, simulations were run for E_{coil}-Dap_{Fur}-1/R_{coil}-Lys-15, E_{coil}-Dap_{Fur}-8/R_{coil}-Lys-8, and E_{coil}-Dap_{Fur}-15/R_{coil}-Lys-1. The probability densities between the Cα atoms of the a_1–a_3, a_2–a_2, and a_3–a_1 residues were plotted against the distance for the antiparallel and parallel orientation (Fig. 5A and B and data in ESI, Fig. S43†). In Fig. 5A, the probability density of the E_{coil}-Dap_{Fur}-1/R_{coil}-Lys-15, when adopting an antiparallel conformation, exhibits a maximum at small distances (below 8 Å), indicating that the antiparallel configuration is very stable. In addition, the probability densities for the a_2–a'_2 and a_3–a'_3 pairs for the parallel configuration (Fig. 5B) exhibit a maximum at longer distances, indicating that the parallel conformation is not stable for this coiled-coil. Finally, the probability density of the number of native contacts *Q* was plotted in Fig. 5C. These data show a clear preference of this coiled-coil for the antiparallel configuration. The same results were also observed for the E_{coil}-Dap_{Fur}-8/R_{coil}-Lys-8 and E_{coil}-Dap_{Fur}-15/R_{coil}-Lys-1.

In order to understand whether the occurrence of an alternative orientation of these heterodimeric E3/R3 coiled-coil pairs in solution was induced by the introduction of modifications (the furan moiety on the E_{coil}, the replacement of Lys by Arg on the K_{coil}, and the Aba group at the N-terminus), FRET measurements were carried out based on pyrene-modified, but otherwise unmodified, coiled-coils.

A pyrene moiety was attached to either the N- or C-terminus of the native E_{coil} and K_{coil} peptides (sequences are reported in Table 3 and data in ESI, Fig.S44–47†). The selection of pyrene as reporter unit was driven by the stronger dependence of its excimer fluorescence emission (formed when two pyrene units are in close proximity) as a function of distance and orientation,[57–59] as compared to other classical FRET pairs that typically have Förster radii in the range of 40 to 100 Å.[60–62]

Table 3 Overview of the sequences of the synthesized pyrene probes. py: 1-pyrene butyric acid that reacted with the side chain amino group of lysine. Ac: acetyl

Name	Sequence
N_{py}-K_{coil}	Py-KIAALKEKIAALKEKIAALKEK(Ac)-NH_2
K_{coil}-C_{py}	Ac-KIAALKEKIAALKEKIAALKEK(Py)-NH_2
N_{py}-E_{coil}	Py-EIAALEKEIAALEKEIAALEKK(Ac)-NH_2
E_{coil}-C_{py}	Ac-EIAALEKEIAALEKEIAALEKK(Py)-NH_2

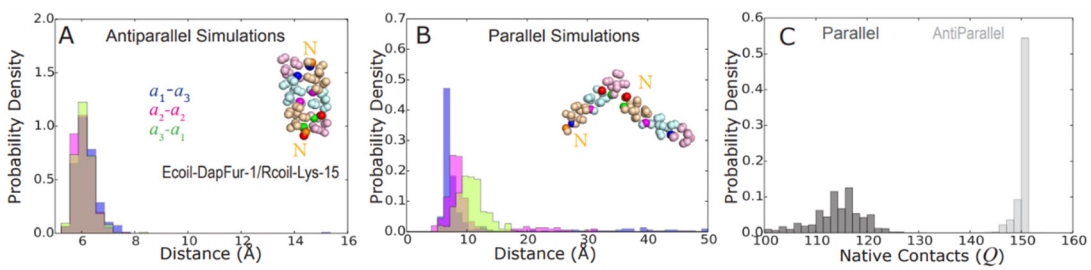

Fig. 5 (A) Probability densities of the distance between the Cα atoms of a_i–a'_i pairs, with i one of the three heptad repeats of the coiled-coil (CC) model in antiparallel orientation. (B) Parallel version of the CC model. Snapshots of the simulations are shown in panels A and B. Each heptad repeat of the CCs is coloured in a different colour: light orange (1st heptad), cyan (2nd heptad), and pink (3rd heptad). The a_i–a_i pair results are represented in the snapshots as blue, magenta, and green bars, respectively. The furan–lysine linkage is represented by the red beads. (C) Probability densities of the number of native contacts *Q*.

In the parallel N_{py}-E_{coil}/N_{py}-K_{coil} heterodimeric coiled-coil system (see Fig. 6A), the two pyrene-modifications are placed on analogous termini, facing each other, at a distance shorter than 10 Å. However, if one of the pyrenes is placed at the N-terminus of one coil and the other at the C-terminus of the second coil (*i.e.* on opposite termini of a parallel coiled-coil structure, see Fig. 6B), the coiled-coil system will keep the two pyrene units apart, at ~32 Å (based on PDB: 1U0I). Therefore, if only a parallel structure is formed, the excimer emission based on pyrene–pyrene stacking should only be observed in the former scenario. The fluorescence emissions of the pyrene-modified K/E_{coil} peptides at the N or C terminus (see Table 3) were evaluated at 5 μM probe concentration in PBS pH 7.4. As shown in Fig. 6C, D and in Fig. S48,† excimer emission (a broad band ranging from 425 nm to 550 nm, centered around 480 nm) was observed for all combinations of peptides, regardless of which peptide terminus was modified with pyrene.

Next, the excimer/monomer emission ratio of coiled-coils pairs was calculated and, in all cases, was higher than the one containing a single probe at double concentration (10 μM, see Fig. 6E). These results demonstrate that there is co-existence of the parallel and antiparallel conformation for the E3/K3 coiled-coil. Moreover, the fluorescence emissions of the pyrene-modified coiled-coils were also recorded after the addition of DMF, which stabilizes the pyrene–pyrene interaction but destabilizes the formation of coiled-coil.[63–65] A reduction of the excimer fluorescence when adding DMF, confirmed that the excimer emission band was observed as a consequence of the coiled-coil formation (see data in ESI, Fig. S48,† panel C and D). In addition, CD analysis showed that the coiled-coil domains are formed for the four possible combinations of pyrene-modified E_{coil} and K_{coil} peptides (Fig. 6F, G and data in ESI, Fig. S49†). Taken together, these results support the existence of a dynamic equilibrium between a parallel and an antiparallel orientation is established in solution.

Next, thermal denaturation experiments were also performed with the pyrene modified probes (Fig. 7). These experiments show that moving from a K_{coil} to R_{coil} resulted in an

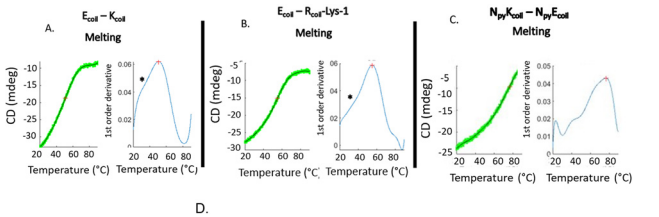

D.

Sample	Tm (°C)	T'_{Trans} (°C)
E_{coil} + K_{coil}	50.8	*
E_{coil} + R_{coil}-Lys-1	55.3	*
$N_{py}K_{coil}$ + $N_{py}E_{coil}$	73.3	47.7*

Fig. 7 Thermal denaturation curves and their 1st order derivative obtained from the equimolar mixture of (A) E_{coil} + K_{coil} (B) E_{coil} + R_{coil}-Lys-1, (C) N_{py}-E_{coil} + N_{py}-K_{coil}. * indicates the presence of a possible transition that does not show a pronounced maximum in the 1st order derivative. (D) Obtained melting temperatures.

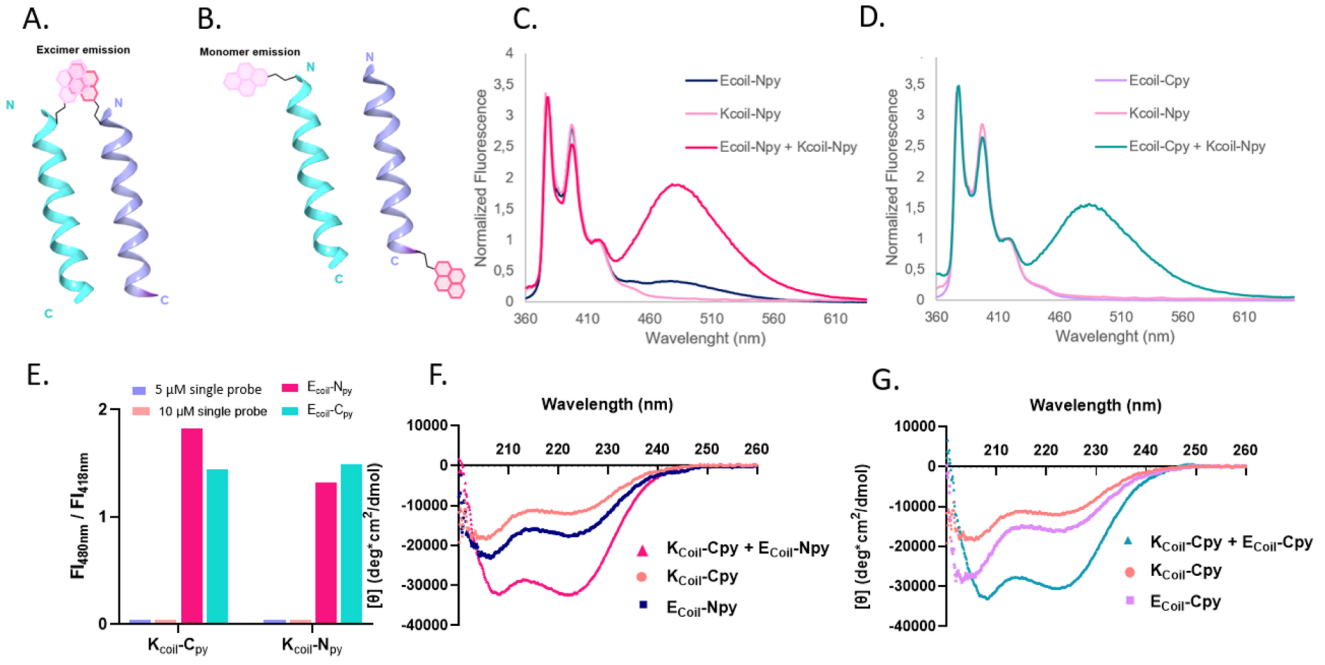

Fig. 6 Cartoon of the orientation of the pyrene-modified coiled-coil systems in case of excimer emission (A) and monomer emission (B). Fluorescence emission spectra of N_{py}-E_{coil} (C) and E_{coil}-C_{py} (D) in presence of N_{py}-K_{coil}. (E) Excimer/monomer emission intensity ratio for the pyrene-modified coiled-coil systems and the single probes. CD data of (F) N_{py}-E_{coil} (dark blue), K_{coil}-C_{py} (orange) and the mixture of the two (pink) (G) E_{coil}-C_{py} (purple), K_{coil}-C_{py} (orange) and the mixture of the two (blue-green). Measurements were performed at 5 μM for each peptide in PBS pH 7.4.

increase in complex stability, with no significant differences based on the position of the lysine residue (see Table S5 and ESI Fig. S50 and S51†). Additionally, these results indicate that the introduction of the pyrene moieties resulted in a drastic increase in complex stability, with increases in the Tm that do not depend on the relative position of the pyrene moieties. In addition, introducing these aromatic moieties allowed a more clear identification of a second transition related to a less stable complex, eventually connected to the presence of both parallel- and antiparallel conformations at room temperature.

Finally, in an attempt to quantify the fractions of parallel- and antiparallel conformations, an alternative crosslinking strategy, earlier developed by us, was applied. In Fig. 2 (*vide supra*), a series of crosslink reactions was shown between the K_{coil} peptide and the different E_{coil}-X_{Fur} peptides. There it can be seen that the broader peak, corresponding to the crosslinked product (and marked with the red circle) is composed of multiple smaller peaks. Indeed, upon applying the furan-oxidation crosslink strategy, in principle all lysine residues that reside in the K_{coil} can react, rendering it impossible to identify which peak corresponds to the parallel or antiparallel orientation. Therefore, in order to allow less ambiguous quantification of the fractions of parallel and antiparallel E3/$K3_1$ coiled-coils, we decided to recur to an alternative crosslinking strategy, earlier described by us (Fig. 8A).[66] Herein, a 5-methylfuran-2-yl moiety that is introduced in the E_{coil} is conveniently converted into a 2,5-dioxopentanyl (2,5-DOP) derivative under peptide cleavage conditions. The DOP function can then be exploited in proximity-induced ligation methodologies with hydrazine nucleophiles. Additionally, this bio-orthogonal ligation, which proceeds under physiological conditions, does not require any stimulus or trigger. With that in mind, K_{coil} and R_{coil} peptide analogues were synthesized containing the hydrazine functionality either at position 1 or 20 (Table 4). Therefore, in the K3/R3 peptides, a hydrazine-modified ornithine residue (Orn_{Hy} in Fig. 8B) replaced the lysine residue at position 1 or 20. In the E3 peptide the glutamic acid residue at position 6 was replaced by a 5-methylfuran-2-yl-modified ornithine which gives rise to a dioxopentanyl moiety upon cleavage of the peptide from the resin (Orn_{DOP}), resulting from acidic hydrolysis of the methylfuran moiety under the cleavage conditions. Next, crosslinking experiments were performed with different hydrazine-K_{coil} and -R_{coil} analogues and the E_{coil}-Orn_{DOP}-6 peptide (Fig. 8). In these experiments, crosslinking was achieved by simply mixing 5 μM of E_{coil}-Orn_{DOP}-6 with 10 μM of R_{coil}/K_{coil} peptide, followed by 2 h of shaking (ESI Fig S57–S64†). After quenching the reaction mixtures at t = 0 h, t = 0.5 h, t = 1 h and t = 2 h with acetone, so that no further crosslinking could take place, HPLC traces were recorded at 214 nm. Based on the disappearance of the signal corresponding to the E_{coil}-Orn_{DOP}-6 and the appearance of the signal corresponding to the crosslinked product, crosslink yields were determined for all combinations as shown in Fig. 8B. In combination with the previous experiments and calculations, additional evidence for a considerable fraction of antiparallel coiled coil is provided.

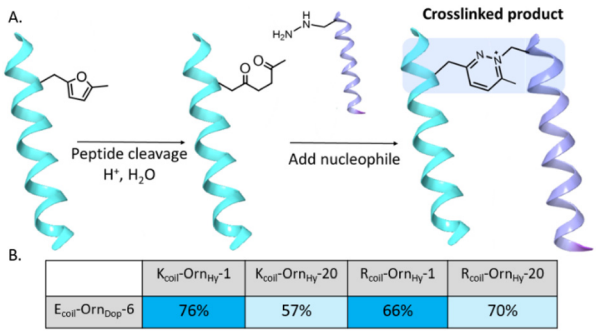

	K_{coil}-Orn_{Hy}-1	K_{coil}-Orn_{Hy}-20	R_{coil}-Orn_{Hy}-1	R_{coil}-Orn_{Hy}-20
E_{coil}-Orn_{DOP}-6	76%	57%	66%	70%

Fig. 8 (A) Cartoon of the dioxopentanyl-hydrazine proximity based crosslinking methodology. (B) Yields for each crosslinked product obtained from the given peptide combinations after 2 h of mixing. The concentration of E_{coil}-Orn_{DOP}-6 peptide was 5 μM and the concentration of the R_{coil} and K_{coil} peptides equalled 10 μM. The dark colors in the table refer to parallel coiled-coils whereas the faded colors represent an anti-parallel coiled-coil. Yields were calculated by integrating signals in the HPLC chromatograms in Fig. S57–64† according to the procedure defined in ESI section 1.5.1.†

Table 4 Overview of the sequences of the synthesized probes. Aba: 4-acetamidobenzoic acid; DOP: 2,5-dioxopentanyl, Hy: hydrazine, Orn: ornithine

Name	Sequence
E_{coil}-Orn_{DOP}-6	Aba-EIAAL-**Orn_{DOP}**-KEIAALEKEIAALEK-NH_2
K_{coil}-Orn_{Hy}-1	Aba-**Orn_{Hy}**-IAALKEKIAALKEKIAALKE-NH_2
K_{coil}-Orn_{Hy}-20	Aba-KIAALKEKIAALKEKIAAL-**Orn_{Hy}**-E-NH_2
R_{coil}-Orn_{Hy}-1	Aba-**Orn_{Hy}**-IAALRERIAALRERIAALRE-NH_2
R_{coil}-Orn_{Hy}-20	Aba-RIAALRERIAALRERIAAL-**Orn_{Hy}**-E-NH_2

Conclusions

In the current work, we studied the use of furan crosslinking to produce covalently crosslinked heterodimeric E3/K3 coiled-coil dimers. Due to the presence of multiple Lys residues on the K_{coil}, which are in close proximity to the furan moiety in the E_{coil}, several crosslinked products were observed. The K_{coil} was once again converted to an R_{coil} to identify which Lys-side chains can react with the furan moiety incorporated at different positions within the E_{coil}. Surprisingly, we observed crosslinking between reacting residues located at opposite sides of the coiled-coil complex, pointing towards the co-existence of an antiparallel orientation of the E3/R3 coiled-coil in solution.

Computational, as well as experimental studies, were performed to validate the co-existence of a parallel and antiparallel orientation of the E3/R3 coiled-coil system. Using a coarse-grained model, various parallel and antiparallel models of crosslinked E3/R3 coiled-coils were studied. Fluorescence measurements based on pyrene–pyrene stacking further supported the double orientation of these heterodimeric E3/K3 coiled-coils in solution. Previously, Franziska Thomas *et al.*

observed different orientations of *de novo* design coiled-coil peptides in their search towards unambiguous heterodimeric coiled-coil dimers.[36] Varying orientations were also occasionally observed in designed protein-based architectures.[52]

With the current experiments, we were now able to firmly demonstrate, the co-existence of both the parallel and antiparallel orientation of the heterodimeric E3/K3 coiled-coil system in solution. The $(EXYZLEK)_3$/$(KXYZLKE)_3$ coiled-coil dimer has been classically considered a parallel system in most of the studies described to date,[17,38] and many of the designed applications are based on this assumption.[25–27,30] The orientation of the coiled-coil strands can be crucial for the sensitivity of many of the developed detection methods (*vide supra*), and becomes even more important when no protein payload is attached. Therefore, we feel that the scientific community can benefit from being aware of the co-existence of parallel and antiparallel conformations when using the $(EXYZLEK)_3$/$(KXYZLKE)_3$ coiled-coil peptide system for a final application. In future investigations and developments based on $(EXYZLEK)_3$/$(KXYZLKE)_3$ coiled-coils both orientations need to be taken into account when designing systems that should generate reliable signals upon their dimerisation.

Author contributions

The authors confirm contribution to the paper as follows: M.d. V. synthesized a first series of R_{Coil} and E_{Coil} peptide analogues. D.S.N resynthesized R_{Coil} and E_{Coil} peptide analogues and optimised the crosslinking experiments. D.A also synthesized the R_{Coil}, E_{Coil} modified peptide analogues, performed crosslinking experiments, CD analysis under the guidance of L.M.C. and contributed to the final version of the manuscript. L.M.C supervised and performed CD analysis. A. Manicardi synthesized pyrene-, DOP-, and hydrazine-modified coils, performed fluorescence experiments, CD experiments, and thermal denaturation experiments. D. G and Y.L did all computational studies. L.M.C, A. Madder and A. Manicardi discussed the results, provided critical feedback, conceived the presented idea, and contributed to the final version of the manuscript. All authors reviewed the results and approved the final version of the manuscript.

Conflicts of interest

There are no conflicts to declare.

Acknowledgements

This work was partially supported by the FWO and the European Union's Horizon 2020 Research and Innovation Programme under the Marie Skłodowska-Curie grant agreement no. 665501, UGent Industrieel Onderzoeksfonds projects F2019/IOF-ConcepTT/188 and F2020/IOF-ConcepTT/111 (Al. M). DA is indebted to the FWO-Vlaanderen for a PhD grant. AM is recipient of a concerted research action grant (MEMCLiP) from Ghent University supporting this research (GOA-028-19). This research was also partially supported by the University of Parma through the action 'Bando di Ateneo 2021 per la ricerca' co-funded by MUR-Italian Ministry of Universities and Research (D.M. 737/2021 – PNR – PNRR – NextGenerationEU) to Al. M. This work has benefited from the equipment and framework of the COMP-HUB and COMP-R Initiatives, funded by the 'Departments of Excellence' program of the Italian Ministry for University and Research (MIUR 2018–2022 and MUR 2023–2027).

References

1 F. H. C. Crick, *Acta Crystallogr.*, 1953, **6**, 685–689.
2 F. H. C. Crick, *Acta Crystallogr.*, 1953, **6**, 689–697.
3 L. Pauling and R. B. Corey, *Nature*, 1953, **171**, 59–61.
4 O. D. Testa, E. Moutevelis and D. N. Woolfson, *Nucleic Acids Res.*, 2009, **37**, D315–D322.
5 A. S. Cristie-David, A. Sciore, S. Badieyan, J. D. Escheweiler, P. Koldewey, J. C. A. Bardwell, B. T. Ruotolo and E. N. G. Marsh, *Mol. Syst. Des. Eng.*, 2017, **2**, 140–148.
6 X. Pan and T. Kortemme, *J. Biol. Chem.*, 2021, **296**, 100558.
7 D. N. Woolfson, in *Adv. Protein Chem*, Academic Press, 2005, pp. 79–112.
8 R. S. Hodges, A. K. Saund, P. C. Chong, S. A. St-Pierre and R. E. Reid, *J. Biol. Chem.*, 1981, **256**, 1214–1224.
9 S. E. Hitchcock-DeGregori and B. Barua, *Subcell. Biochem.*, 2017, **82**, 253–284.
10 K. T. O'Neil and W. F. Degrado, *A thermodynamic scale for the helix-forming tendencies of the commonly occurring amino acids*, 1990, vol. 250, pp. 646–651.
11 B. Lovejoy, S. Choe, D. Cascio, D. K. McRorie, W. F. DeGrado and D. Eisenberg, *Science*, 1993, **259**(5099), 1288–1293.
12 C. P. Hill, D. H. Anderson, L. Wesson, W. F. DeGrado and D. Eisenberg, *Science*, 1990, **249**, 543–546.
13 A. N. Lupas and J. Bassler, *Trends Biochem. Sci.*, 2017, **42**, 130–140.
14 D. N. Woolfson, in *Fibrous Proteins Struct. Mech*, ed. D. A. D. Parry and J. M. Squire, Springer International Publishing, Cham, 2017, pp. 35–61.
15 A. N. Lupas and M. Gruber, in *Adv. Protein Chem*, Academic Press, 2005, pp. 37–38.
16 J. Walshaw and D. N. Woolfson, *Protein sci.*, 2001, **10**, 668–673.
17 J. R. Litowski and R. S. Hodges, *J. Biol. Chem.*, 2002, **277**, 37272–37279.
18 Y. Yano, A. Yano, S. Oishi, Y. Sugimoto, G. Tsujimoto, N. Fujii and K. Matsuzaki, *ACS Chem. Biol.*, 2008, **3**, 341–345.
19 R. R. Naik, S. M. Kirkpatrick and M. O. Stone, *Biosens. Bioelectron*, 2001, **16**(9–12), 1051–1057.
20 H. Chao, D. L. Bautista, J. Litowski, R. T. Irvin and R. S. Hodges, *J. Chromatogr. B: Biomed. Sci. Appl.*, 1998, **715**, 307–329.

21 W. M. Rink and F. Thomas, *Chem. – Eur. J.*, 2019, **25**, 1665–1677.
22 P. Wolf, G. Gavins, A. G. Beck-Sickinger and O. Seitz, *ChemBioChem*, 2021, **22**, 1717–1732.
23 Y. Yano and K. Matsuzaki, *Biochim. Biophys. Acta, Biomembr.*, 2019, **1861**, 1011–1017.
24 G. C. Gavins, *Nat. Chem.*, 2021, **13**(1), 15–23.
25 H. Yamashita, Y. Yano, K. Kawano and K. Matsuzaki, *Biochim. Biophys. Acta, Biomembr.*, 2015, **1848**, 1359–1366.
26 J. Utterström, S. Naeimipour, R. Selegard and D. Aili, *Adv. Drug Delivery Rev.*, 2021, **170**, 26–43.
27 K. Kawano, Y. Yano, K. Omae, S. Matsuzaki and K. Matsuzaki, *Anal. Chem.*, 2013, **85**(6), 3453–3461.
28 M. M. Stevens, N. T. Flynn, C. Wang, D. A. Tirrell and R. Langer, *Adv. Mater.*, 2004, **16**, 915–918.
29 Y. Wu and J. H. Collier, *Wiley Interdiscip. Rev.: Nanomed. Nanobiotechnol.*, 2017, **9**, e1424.
30 B. Liberelle, L. Bartholin, C. Boucher, F. Murschel, M. Jolicoeur, Y. Durocher, A. Merzouki and G. De Crescenzo, *J. Immunol. Methods*, 2010, **362**, 161–167.
31 J. Wang, Y. Yu and J. Xia, *Bioconjugate Chem.*, 2014, **25**, 178–187.
32 S. H. Hong, T. Nguyen and P. Arora, *Curr. Protoc.*, 2022, **2**, e315.
33 M. G. Wuo, A. B. Mahon and P. S. Arora, *J. Am. Chem. Soc.*, 2015, **137**, 11618–11621.
34 A. S. Eklund, M. Ganji, G. Gavins, O. Seitz and R. Jungmann, *Nano Lett.*, 2020, **9**, 6732–6737.
35 E. K. O'Shea, J. D. Klemm, P. S. Kim and T. Alber, *Science*, 1991, **254**, 539–544.
36 F. Thomas, A. L. Boyle, A. J. Burton and D. N. Woolfson, *J. Am. Chem. Soc.*, 2013, **135**, 5161–5166.
37 M. D. Watson, I. Peran and D. P. Raleigh, *Biochemistry*, 2016, **55**, 3685–3691.
38 D. A. Lindhout, J. R. Litowski, P. Mercier, R. S. Hodges and B. D. Sykes, *Biopolymers*, 2004, **75**, 367–375.
39 T. Zheng, A. Boyle, H. R. Marsden, D. Valdink, G. Martelli, J. Raap and A. Kros, *Org. Biomol. Chem.*, 2015, **13**, 1159–1168.
40 E. A. Golysheva, A. L. Boyle, B. Biondi, P. Ruzza, A. Kros, J. Raap, C. Toniolo, F. Formaggio and S. A. Dzuba, *Biochemistry*, 2021, **60**, 19–30.
41 L. L. G. Carrette, E. Gyssels, N. De Laet and A. Madder, *Chem. Commun.*, 2016, **52**, 1539–1554.
42 M. Op de Beeck and A. Madder, *J. Am. Chem. Soc.*, 2012, **134**, 10737–10740.
43 C. Véliz Montes, H. Memczak, E. Gyssels, T. Torres, A. Madder and R. J. Schneider, *Langmuir*, 2017, **33**, 1197–1201.
44 A. Manicardi, E. Cadoni and A. Madder, *Chem. Sci.*, 2020, **11**, 11729–11739.
45 A. Manicardi, E. Gysels, R. Corradini and A. Madder, *Chem. Commun.*, 2016, **52**, 6930–6933.
46 W. Vannecke, C. Ampe, M. Van Troys, M. Beltramo and A. Madder, *ACS Chem. Biol.*, 2017, **12**, 2191–2200.
47 L. Miret-Casals, W. Vannecke, K. Hoogewijs, G. Arauz-Garofalo, M. Gay, M. Dı´az-Lobo, M. Vilaseca, C. Ampe, M. Van Troys and A. Madder, *Chem. Comm.*, 2021, **57**, 6054–6057.
48 L. Miret-Casals, S. Van De Putte, D. Aerssens, J. Diharce, P. Bonnet and A. Madder, *Front. Chem.*, 2022, **9**, 799706.
49 V. N. Malashkevich, C. D. Higgins, S. C. Almo and J. R. Lai, *Biopolymers*, 2015, **104**, 178–185.
50 O. D. Monera, N. E. Zhou, P. Lavigne, C. M. Kay and R. S. Hodges, *J. Biol. Chem.*, 1996, **271**, 3995–4001.
51 D. J. Glover, S. Lim, D. Xu, N. B. Sloan, Y. Zhang and D. S. Clark, *ACS Synth. Biol.*, 2018, **7**, 2447–2456.
52 T. Zheng, M. Bulacu, G. Daudey, F. Versluis, J. Voskuhl, G. Martelli, J. Raap, G. J. A. Sevink, A. Kros and A. L. Boyle, *RSC Adv.*, 2016, **6**, 7990–7998.
53 M. G. Wuo, S. H. Hong, A. Singh and P. S. Arora, *J. Am. Chem. Soc.*, 2018, **140**, 16284–16290.
54 D. Gomez, Y. Gavrilov and Y. Levy, *Biophys. J.*, 2019, **116**, 1228–1238.
55 S. Y. Lau, A. K. Taneja and R. S. Hodges, *J. Biol. Chem.*, 1984, **259**, 13253–13261.
56 P. Burkhard, M. Meier and A. Lustig, *Protein Sci. Publ. Protein Soc.*, 2000, **9**, 2294–2301.
57 A. Manicardi, A. Bertucci, A. Rozzi and R. Corradini, *Org. Lett.*, 2016, **18**, 5452–5455.
58 G. Bains, A. B. Patel and V. Narayanaswami, *Molecules*, 2011, **16**, 7909–7935.
59 G. K. Bains, S. H. Kim, E. J. Sorin and V. Narayanaswami, *Biochemistry*, 2012, **51**, 6207–6219.
60 J. Breidenbach, U. Bartz and M. Guetschow, *Biochim. Biophys. Acta, Proteins Proteomics*, 2020, **1868**, 140445.
61 B. T. Bajar, E. S. Wang, S. Zhang, M. Z. Lin and J. Chu, *Sensors*, 2016, **16**, 1488.
62 Y. Arai and T. Nagai, *Microscopy*, 2013, **62**, 419–428.
63 M. Masuko, H. Ohtani, K. Ebata and A. Shimadzu, *Nucleic Acids Res.*, 1998, **26**, 5409–5416.
64 C. Mattos and D. Ringe, *Curr. Opin. Struct. Biol.*, 2001, **11**, 761–764.
65 T. Knubovets, J. J. Osterhout and A. M. Klibanov, *Biotechnol. Bioeng.*, 1999, **63**, 242–248.
66 A. Manicardi, E. Cadoni and A. Madder, *Commun. Chem.*, 2021, **4**, 1–9.